Prediction of process-induced void formation in anisotropic Fiber-reinforced autoclave composite parts

As Published: https://doi.org/10.1007/s12289-019-01477-4

Publisher: Springer Paris

Persistent URL: https://hdl.handle.net/1721.1/131798

Version: Author's final manuscript: final author's manuscript post peer review, without publisher's formatting or copy editing

Prediction of Process-Induced Void Formation in Anisotropic Fiber-Reinforced Autoclave Composite Parts

Bamdad Barari[1], Pavel Simacek[*, 2] Shridhar Yarlagadda[*, 3], Roger M. Crane[*, 3]

and Suresh G Advani[*, 2]

Massachusetts Institute of Technology[1], Boston, MA

Department of Mechanical Engineering[2] and Center for Composite Materials[*]

University of Delaware

Composites Automation LLC[3]

Newark, DE

Abstract

A numerical methodology is proposed to predict void content and evolution during autoclave processing of thermoset prepregs. Starting with the initial prepreg void content, the void evolution model implements mechanisms for void compaction under the effect of the applied pressure, including Ideal Gas law compaction, and squeeze flow for single curvature geometries. Pressure variability in the prepreg stack due to interactions between applied autoclave pressure and anisotropic material response are considered and implemented. A parametric study is conducted to investigate the role of material anisotropy, initial void content, and applied autoclave pressure on void evolution during consolidation of prepregs on a tool with single curvatures. The ability of the model to predict pressure gradient through the thickness of the laminate and its impact on void evolution is discussed.

1. Introduction

One of the traditional methods to fabricate composites is using prepreg layups. Prepregs contain reinforcing unidirectional fibers or woven fabrics that are preimpregnated with either a thermoplastic or thermoset resin. If a thermoset matrix is used, the resin is partially cured for ease of handling and this b-stage prepreg must be heated in an oven or an autoclave for consolidation and complete cure [1]. Composite parts can be made from such prepregs by stacking them, heating the assembly, curing and consolidating them under pressure. Autoclave prepreg processing is one of the composite manufacturing methods typically used for high-end structural applications especially in the aerospace industry, since it provides excellent

[1] Corresponding author's email: bbarari@mit.edu

mechanical characteristics with good reproducibility [2]. Moreover, the material behavior can be tailored by using unidirectional prepregs that can be stacked in the required orientation sequence, with the resin system tailored for the specific application by adding additives, such as flame retardants, or toughening agents, in order to meet specific requirements. Flat laminates or structures can be reliably made with this process without any anomalies such as wrinkles or other defects [3].

For complex geometry parts with prepreg stacks, manufacturing defects such as porosity, possible wrinkling and reinforcement disorientation which introduce gaps and overlaps within the laminate, will detrimentally affect the final mechanical properties (stiffness, strength) of the component being constructed especially for parts that have single and/or double curvature [4-9]. Curved cross-sectional laminate parts are very diverse in design including, T-shaped, L-shaped, J-shaped parts. The L-shaped part is one of the simplest designs of complex structures and is extensively used in the aircraft industry. Several experimental and numerical papers have been published regarding the compaction quality of the parts using the autoclave process [10-15]. The effect of the processing parameters, such as cure cycle, mold design, bagging configuration and stacking sequence have been investigated to some extent [16, 17]. Several models have been developed to predict composite resin flow in autoclave processing [18-25]. These studies were mainly focused on the consolidation of simple shaped laminates. Hubert et al. [19] and Li and Tucker [24] developed and implemented a finite element-based flow-compaction model for L shaped composite laminates. Hubert et al. [19] used an incremental, quasi-linear elastic finite element model to simulate the multiple physical phenomena in autoclave processing. Li and Tucker [24] developed a hyper-elastic model for fiber reinforcement stress where the mesh geometry and fiber orientation were updated during the consolidation process. Dong [25] developed a model for predicting the formation of the resin-rich zone in angled composite laminates. Dong's model quantitatively related gap thickness with the radius, fiber volume fraction, stacking sequence and enclosed angle. Gutowski et al. [22] proposed a 3D flow and a 1D compaction model and characterized the composite as a deformable unidirectional fiber reinforced structure where the load is balanced by the average resin pressure and the average effective stress in the fiber network. Dave et al. [21] used a similar approach but their model considered the flow in different directions to be coupled. However, the effect of compaction pressure and its interaction with the void content has not been addressed especially for part

geometries with curvature. The evolution of void content during processing and sensitivity to complex interactions between the locally applied pressure and the non-uniform resin pressure experienced by the resin within the prepreg plies needs to be investigated.

In the present study, a pressure model is developed to predict through thickness resin pressure distribution and the consolidation stress components on a ply-by-ply basis for an L-shaped geometry. Ply-by-ply void content is tracked and void evolution during processing is modeled considering void compaction due to pressure (Ideal Gas law) and squeeze flow of resin into voids. Constitutive equations are developed to describe the anisotropic material behavior of the prepreg as well as the stress-strain relation which accounts for the resin pressure term due to the squeeze flow and Ideal Gas law compaction. The model is fully coupled with the ABAQUS solver through an UMAT subroutine. This ABAQUS integrated approach allows one to import complex geometries, establish process conditions and address local void evolution due to non-uniform resin pressure at corners or in specific complex geometry zones.

2. Model development and mechanisms

In a typical autoclave process, thermoset prepreg layers are processed at elevated temperature and pressure. Vacuum is drawn on the part to remove volatiles that can be removed that way, temperature is raised to reduce resin viscosity and pressure is build up to dissolve more volatiles and fill the empty pores with resin. Finally, temperature – and sometimes pressure, too - are elevated even more to cure the resin. Consolidating pressure is applied through a compliant bag against the tool surface. Additional steps may be involved in the process. For example, thick layup stacks may be incrementally “debulked” under vacuum several times during the layup to reduce the content of trapped volatiles. While this does not necessarily change the consolidation process, the amount of volatiles to be disposed of is significantly reduced that way.

Thus, as the temperature and pressure varies during the process, the material behavior has to be properly described as a function of temperature and pressure to properly describe consolidation and the initial porosity and void content should be reasonably described. These steps go beyond the scope of this work and we will, optimistically, assume that they can be accomplished to full satisfaction.

At the beginning of the process, the stacked prepregs contain significant voids and potentially, volatiles such as moisture. Additional porosity may also develop during the process because (i) the increase in temperature may evaporate the liquid volatiles in the system and (ii)

curing reaction may release by-products in gaseous state, however these effects are not being considered at this time.

During the consolidation process, the void content within the composite should be reduced to acceptable (~1 to 2% for aerospace components) range, which is generally accomplished by subjecting the prepreg assembly to higher applied pressures. The resin pressure in the system during the consolidation is not the sole force to carry the applied autoclave pressure. Consolidation requires volumetric and shape change of the prepreg stack and under this deformation the fibrous bed within the prepreg develops the stress field and carries part of the applied load. This combined with the resin pressure, according to the Terzaghi equation, is equal to the total applied consolidation pressure. Consequently, the resin pressure will always be less than the applied consolidation pressure and an understanding of the mechanisms that determine resin pressure as a function of incoming material characteristics, geometry, and process conditions is critical.

The resultant resin pressure can reduce void content by the following mechanisms

- Void size reduction due to volatile gas compression by the higher external resin pressure than internal void pressure – Ideal Gas law-based compression
- Void size reduction by driving resin flow into voids from neighboring regions
- Dissolution of void gas into resin driven by solubility (Henry's Law)
- Diffusion mechanisms enabling transport of dissolved species to the surface of the prepreg stack, typically driven by concentration gradients and thus related with the dissolution

Note that the pressure in voids needs to be lower than the resin pressure for all these mechanisms to occur. As thermoset prepreg is typically stored under ambient pressure conditions, the general assumption is that the initial internal void pressure is in equilibrium with atmospheric pressure prior to autoclave processing.

The unidirectional fibers (e.g. carbon or glass) within each prepreg layer make the prepreg properties highly anisotropic. The transverse compliance is relatively high for such prepreg layers with the in-plane stiffness in fiber direction being orders of magnitude larger. The latter plays an important role in curved regions as the membrane stresses can carry a part of the transverse compaction pressure from the autoclave, if fibers are oriented along the curve and may require significant strain in fiber direction or sliding between layers to enable thickness

reduction during compaction. Note that this is specific to concave geometries, where compaction requires either extension or layer sliding due to increase in radius. On the other hand, convex geometries undergo decrease in effective radius and consequent compression along the ply direction. This is the primary cause for wrinkling defects, and is not a focus of this paper.

A resin with significant porosity is not incompressible. The voids (bubbles) within resin contain certain amount of volatiles at some pressure (volatile pressure) which is related to the volume and the amount of captured gas. Change of volatile volume (porosity), pressure (volatile pressure) and mass is linked, say through ideal gas law though other constitutive relation may be used.

The pressure in the resin is coupled with the volatile pressure in the voids. Increase the resin pressure, the porosity gets compressed (and mass gets dissolved) and the volume decreases. Thus, the entire system acts like a progressively stiffening spring which reaches the incompressibility only when the porosity vanishes. Note that the resin pressure varies with location and is not identical to volatile pressure even if the surface tension in voids is neglected. If the voids are large and embedded in the fibrous bed, filling them with resin requires additional pressure to transfer ("flow") the resin from locations without voids to those containing voids. This adds a potentially significant viscous "damper" to the behavior. Relative motion of resin ("squeeze flow") through the reinforcement needed to fill the void regions is modeled using Darcy's law, and has been shown to require significant pressure and/or time to complete.

The above approach focuses on calculation of the resin pressure around voids which will be lower than the applied autoclave pressure due to the fiber bed carrying part of the applied load. Low resin pressure due to poor pressure translation is not desirable but it happens non-uniformly especially around curved geometries. This can promote the evolution of voids within the resin due to insufficient resin pressure.

To address the prediction of resin pressure within the layers of a complex geometry part, three components of the stress field that influence the deformation need to be modeled. First, the reinforcement stress-deformation relation due to the elastic, elasto-plastic, or viscoelastic anisotropic stress needs to be included depending on the material type. Second, the average pressure within the liquid resin has to be related to the volumetric deformation of the resin which is affected by the void hydrostatic pressure developed during the compaction/consolidation process and, consequently, the volatile concentration for the dissolution/diffusion process. To

this one should add pressure increase necessary to transfer the resin to where it is needed (squeeze flow). Lastly, for any curved structure, the reaction between layers will influence the stress field within the reinforcement as it generates in-plane stresses which, for curved surface, influences the transverse momentum conservation. Note that practically, the in-plane stiffness in the fiber direction tends to be *very* significant and this effect is hardly negligible.

In this work, we address two of the above-mentioned three mechanisms. The first mechanism of stress deformation is described by anisotropic elasticity. The second mechanism relates the non-linear elastic component to the compression of voids and has a viscous component which in accordance with Darcy's flow redistributes the resin. The former utilizes ideal gas state equation for the volatiles. The latter brings dependency on the mean spacing of the voids, resin viscosity and permeability of the reinforcing bed. The third mechanism of sliding between layers is not considered as a laminate description was used for the cases we investigated, and shear deformation is employed as the sole mechanism for the relative displacement of the layers. Sliding or partial sliding – whether Coulombian or viscous – is not allowed in our model. This is equivalent to mechanical interlocking of plies which would provide sufficient "static friction." This is a significant simplification but qualitatively it provides the in-plane stress field. The scope of this work is to investigate the effect of anisotropy and voids during the consolidation of curved parts in an autoclave process on final void content in the composite. Summary of the main mechanisms that been used in the model are presented in Table 1.

Table 1. Summary of the actual mechanism and the mechanism we used in model

	Actual autoclave process	**Proposed model assumption**
Prepreg model Reinforcement	Viscoelastic anisotropic response from reinforcement	Linearly elastic anisotropic reinforcement behavior
Prepreg model Resin pressure	▪ Resin pressure caused by hydrostatic pressure in voids ▪ Additional resin pressure caused by resin redistribution (squeeze flow)	▪ Ideal gas law ▪ 1D Darcy squeeze flow ▪ Terzaghi equation used to combine pressure and stress in fiber bed
Interface model	▪ Viscous Resin Interface (Viscous) and dry Friction (Plastic) ▪ Failure/Initial Friction Before Relative Motion Can Occur ▪ Shear deformation both before the initial	▪ Shear deformation is the dominant mechanism in compaction process ▪ No sliding is considered due to the laminate assumption

	failure and after	
Dissolution model	▪ Dissolution of void gas into resin driven by solubility (Henry's Law)	▪ No dissolution of void gas into resin driven by solubility (Henry's Law)
Diffusion model	▪ Diffusion mechanisms enabling transport of dissolved species to the surface of the prepreg	▪ No diffusion is considered

2.1. Elastic behavior of fibrous reinforcement

The first mechanism can be described through the anisotropic elasticity for the fibrous reinforcement in the prepreg. For real materials, this is a rather complex relation. In the scope of this work we opted for simple but anisotropic linearly elastic material, as the goal is to understand the effect of the degree of anisotropy on resin pressure and ultimately void content in complex geometries. The fibrous bed is assumed to behave linearly and exhibits different material properties (i.e., elastic modulus and Poisson's ratio) in the transverse and fiber directions. Therefore, nine material properties ($E_1, E_2, E_3, \nu_{12}, \nu_{13}, \nu_{23}, G_{12}, G_{13}, G_{23}$) are needed to define the linear anisotropic elastic material.

$$\begin{Bmatrix} \sigma_{11} \\ \sigma_{22} \\ \sigma_{33} \\ \sigma_{12} \\ \sigma_{13} \\ \sigma_{23} \end{Bmatrix} = \begin{bmatrix} C_{1111} & C_{1122} & C_{1133} & 0 & 0 & 0 \\ & C_{2222} & C_{2233} & 0 & 0 & 0 \\ & & C_{3333} & 0 & 0 & 0 \\ & sym & & C_{1212} & 0 & 0 \\ & & & & C_{1313} & 0 \\ & & & & & C_{2323} \end{bmatrix} \begin{Bmatrix} \varepsilon_{11} \\ \varepsilon_{22} \\ \varepsilon_{33} \\ \varepsilon_{12} \\ \varepsilon_{13} \\ \varepsilon_{23} \end{Bmatrix} \tag{1}$$

With

$$\begin{aligned} C_{1111} &= E_1(1-\nu_{23}\nu_{32})\gamma \\ C_{2222} &= E_2(1-\nu_{13}\nu_{31})\gamma \\ C_{3333} &= E_3(1-\nu_{12}\nu_{21})\gamma \\ C_{1122} &= E_1(\nu_{21}+\nu_{31}\nu_{23})\gamma \\ C_{1133} &= E_1(\nu_{31}+\nu_{21}\nu_{32})\gamma \\ C_{2233} &= E_2(\nu_{32}+\nu_{12}\nu_{31})\gamma \\ C_{1212} &= G_{12} \\ C_{1313} &= G_{13} \\ C_{2323} &= G_{23} \\ \gamma &= 1/(1-\nu_{23}\nu_{32}-\nu_{31}\nu_{13}-\nu_{12}\nu_{21}-2\nu_{21}\nu_{32}\nu_{13}) \end{aligned} \tag{2}$$

where E_1 and E_2 are the modulus in the fiber direction and transverse in-plane direction respectively, E_3 is the modulus normal to the plane of fiber bed, $\nu_{12}, \nu_{13}, \nu_{23}$ are the Poisson's ratio and G_{12}, G_{13}, G_{23} are the shear moduli in the fiber and the transverse directions respectively. The other three Poisson ratios, ν_{21}, ν_{31} and ν_{32} can be calculated as

$$\nu_{21} = \frac{E_2}{E_1}\nu_{12}$$
$$\nu_{31} = \frac{E_3}{E_1}\nu_{13} \qquad (3)$$
$$\nu_{32} = \frac{E_3}{E_2}\nu_{23}$$

2.2. Modeling the average resin pressure field

The resin itself is, for the loads considered herein, incompressible. It can carry unlimited and indeterminate hydrostatic pressure to be added to the elastic force. However, the volatile voids within the resin are compressible. Thus, for the second mechanism, volatiles resist compaction by developing hydrostatic pressure related to their compression. This pressure translates to resin pressure within the composite prepreg. If resin is available around the voids, the resin pressure on the void interface can be assumed to be the pressure in the volatiles, the resin is essentially in a hydrostatic state and does not move relative to the fiber bed. The existing models tend to add a viscous delay as the fluid shell around the void must deform, but the characteristic times of such process are so low that there is no need to consider it for the autoclave consolidation. However, for the resin to fill the voids insulated from the resin rich areas by the fiber bed, a pressure gradient must develop to squeeze and drive the resin from these areas to resin starved areas by the local relative motion of the resin through the fiber bed. Thus, the average resin pressure will need to be larger than the hydrostatic pressure in the voids. The squeeze flow is induced due to the compaction of the reinforcement layers which creates a higher pressure and a pressure gradient between the voids which will drive the resin into the voids as governed by Darcy's law. This increases the average resin pressure above the "boundary" value in the voids. The effect of this phenomenon is that the consolidation is a transient process, despite the pressure in the voids and the stress field in fiber bed being purely elastic.

Note that should the diffusion and dissolution be modeled (not considered in our model), Henry's law should still be applied using the resin pressure at the interface with the void, not the

averaged resin pressure. As the squeeze flow related pressure gradient builds fast [26], this issue should be considered even on length scales as small as 10 fiber diameters (0.1 mm). Generally, the void spacing is restricted by the ply thickness, so that it likely remains in the sub-millimeter range. The two mechanisms for the pressure in case of stationary situation and the moving resin are shown in Figure 1.

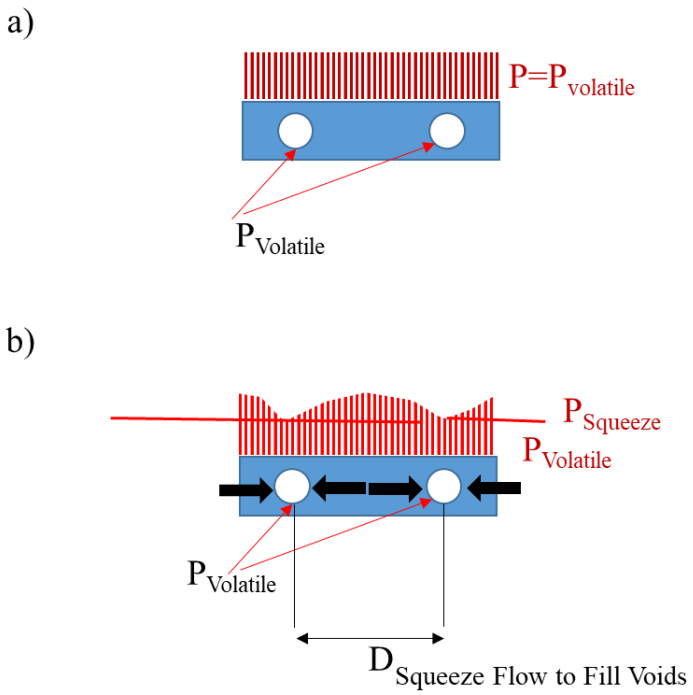

Figure 1. A schematic showing pressure in the resin for a) the hydrostatic and b) hydrostatic and the squeeze flow model.

Through the schematic shown in Figure 1, the average resin pressure consists of two terms as

$$\bar{P} = \bar{P}_{hydrostatic} + \bar{P}_{squeeze} \tag{4}$$

In order to define the hydrostatic pressure term, we can start with the ideal gas law for the volatiles pressure, so the resin pressure could be defined as

$$\bar{P}_{hydrostat} = \frac{P_0 \varphi_0}{\varphi_0 + \varepsilon_{bulk}} \left(\frac{T}{T_{ref}} \right) (1 - d_v) \tag{5}$$

where, P_0 is volatile initial pressure, φ_0 is the initial void fraction, T and T_{ref} are the current temperature and the reference temperature, ε_{bulk} is the bulk strain (usually negative in

consolidation) and d_v is the fraction of original volatiles (in mass or molar terms) that is removed from voids (usually dissolved) during the consolidation process. In non-trivial cases, both the temperature development and volatile dissolution and diffusion need to be tracked independently. This will also bring a transient character to an otherwise purely elastic equation, even if squeeze flow is not considered. The squeeze flow could be added as a second term using the pressure development term,

$$\bar{P}_{squeeze} = \frac{1}{12}\frac{\eta(T)}{K(\varepsilon_{bulk})} D^2 \dot{\varepsilon}_{bulk} \qquad (6)$$

where, $\eta(T)$ is the resin viscosity as a function of the temperature (and time), D is the distance between the voids, $\dot{\varepsilon}_{bulk}$ is the bulk strain rate ("squeeze" rate) that can be in practical implementation defined as strain increment over time increment Δt and $K(\varepsilon_{bulk})$ is the permeability as a function of the bulk strain which can be measured and fitted, or computed from a constitutive equation as

$$K(\varepsilon_{bulk}) = K_0 \frac{(1-\frac{v_{f0}}{1+\varepsilon_{bulk}})^3}{\frac{v_{f0}}{(1+\varepsilon_{bulk})^2}} \qquad (7)$$

Eqn. (7) is Kozeny-Carman empirical equation in which the fiber volume fraction is evaluated from bulk strain and the Kozeny-Carman constant is converted to permeability K_0 which is the value of the permeability at the initial fiber volume fraction v_{f0}. Substituting Eqn. (7) into Eqn. (6) and using the definition for hydrostatic and squeeze flow terms for the average resin pressure, Eqn. (4) could be re-written as

$$\bar{P} = \frac{P_0\varphi_0}{\varphi_0 + \varepsilon_{bulk}}\left(\frac{T}{T_{ref}}\right)(1-d_v) + \frac{{v_{f0}}^2 D^2}{12K_0}\eta(T)\frac{1+\varepsilon_{bulk}}{(1+\varepsilon_{bulk}-v_{f0})^3}\dot{\varepsilon}_{bulk} \qquad (8)$$

As both the void spacing D and permeability K_0 depend on orientation and precise location, these factors (respectively the non-dimensional number D^2/K_0) are the "equivalent" void spacing and permeability. In actual model, the coefficient must be taken as material parameter to determine to achieve best match between model and reality. More accurate

modeling is possible, but it would require very detailed information on void distribution and size, not just porosity and spacing or typical size on length scale *below* the actual consolidation model size. Also note that the squeeze flow model is purely viscous and given sufficient time this component will become insignificant. Thus the characteristic time is important, because if the characteristic value is small, the final state will not be influenced much by this term. On the other hand, should the characteristic time be too long, the resin will gel increasing the viscosity exponentially before the steady state is reached. This may be important in practical situation if one wishes to use the simpler steady state prediction to estimate the consolidation levels.

3. Constitutive model

The linear anisotropic constitutive model, Eqn. (1) is combined with the average resin pressure in Eqn. (8) and used to define the stress-strain relation. In the proposed model, stress is related to strain and also the strain rate through the addition of the pressure term to the constitutive equation as

$$\sigma_{ij} = C_{ijmn}.\varepsilon_{mn} - \delta_{ij}\bar{P} \qquad (9)$$

where C_{ijmn} is a forth order tensor defined by Eqn. (1) for an anisotropic material and δ_{ij} is the tensor index notation of Kronecker delta. Substituting Eqn. (8) into Eqn. (9), stress term can be written as follow

$$\sigma_{ij} = C_{ijmn}.\varepsilon_{mn} - \delta_{ij}\frac{P_0\varphi_0}{\varphi_0+\varepsilon_{kk}}\left(\frac{T}{T_{ref}}\right)(1-d_v) - \delta_{ij}\frac{{v_{f0}}^2 D^2}{12K_0}\eta(T)\frac{1+\varepsilon_{kk}}{(1+\varepsilon_{kk}-v_{f0})^3}\dot{\varepsilon}_{kk} \qquad (10)$$

Note that while D^2/K_0 is "effective" value representing material and process parameter, the characteristic value obtain by averaged spacings/principal permeabilities should provide a decent estimate for this value.

In the finite element model, the UMAT (User-defined Material model in ABAQUS) is developed to calculate the anisotropic modulus and the Jacobian matrix (incremental stiffness tensor) corresponding to the stress state at each iteration. The UMAT allows the user to implement a specific constitutive model other than the default model used by ABAQUS. The ABAQUS standard solver uses the iterative method with the corresponding UMAT to solve the constitutive equations. The iterations continue on the basis of the previous solutions, until a reasonable convergence is reached. The Jacobian matrix (C) is defined as

$$C = \frac{\partial \Delta \sigma}{\partial \Delta \varepsilon} \tag{11}$$

where C is the Jacobian matrix (incremental stiffness matrix); $\partial \Delta \sigma$ is the increment in stress; and $\partial \Delta \varepsilon$ is the increment in strain. Regarding the new definition for stress term presented by Eqn. (10), stress increment as a function of strain increment is defined as

$$\begin{aligned} d\sigma_{ij} = C_{ijmn}\, d\varepsilon_{mn} + \frac{P_0 \varphi_0}{(\varphi_0 + \varepsilon_{kk})^2}\left(\frac{T}{T_{ref}}\right)(1-d_v)\,\delta_{ij} d\varepsilon_{kk} \\ + \frac{{v_{f_0}}^2 D^2}{12K_0}\eta(T)\left(\frac{v_{f_0} + 2(1+\varepsilon_{kk})}{(1+\varepsilon_{kk} - v_{f_0})^4}\right)\dot{\varepsilon}_{kk}\,\delta_{ij} d\varepsilon_{kk} - \frac{{v_{f_0}}^2 D^2}{12K_0}\eta(T)\frac{1+\varepsilon_{kk}}{(1+\varepsilon_{kk} - v_{f_0})^3.\Delta t}\delta_{ij} d\varepsilon_{kk} \end{aligned} \tag{12}$$

The flowchart of the UMAT developed based on constitutive model is shown in Figure 2. Within the UMAT, initial volatile pressure and void distribution, viscosity and material parameters are provided as input and the Jacobian matrix (incremental stiffness matrix) is calculated, then the total stress state is updated using the stress derivative defined by Eqn. (12) and the pressure field which is stored as the state variable in the UMAT. After that, the stress state is returned to the ABAQUS solver for pressure and void evolution. Finally, voids content is updated based on updated strain and pressure data with Ideal gas law and stored as a state variable obtained as follow

$$\varphi = (\varphi_0 + \varepsilon_{bulk}) \tag{13}$$

note that, ε_{bulk} is the negative term which demonstrates the change in thickness due to the laminate compaction during the process.

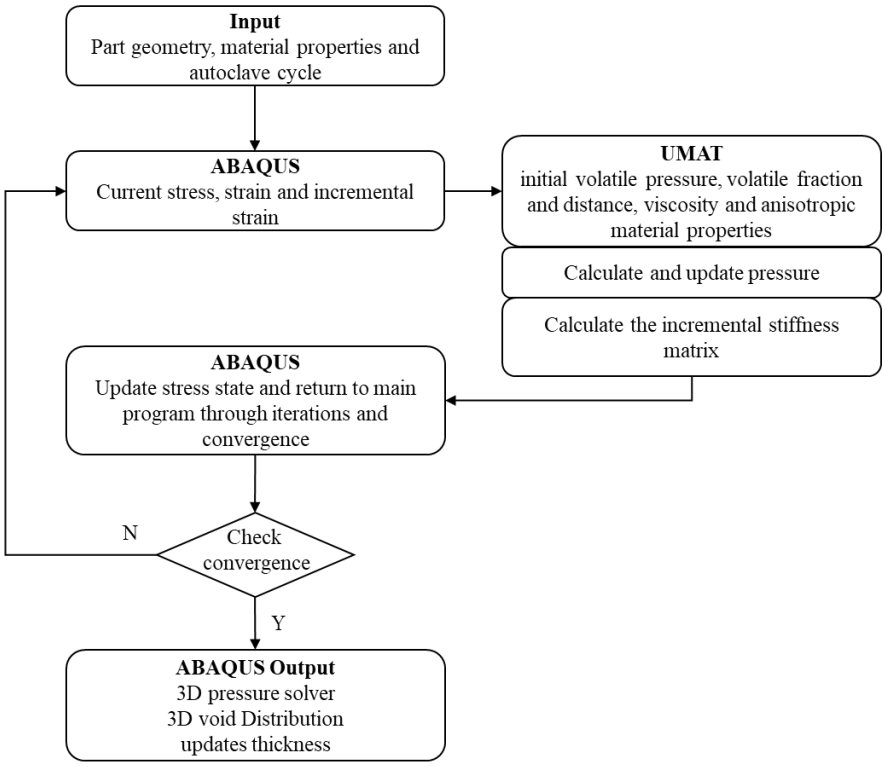

Figure 2. Flowchart of the UMAT integrated with ABAQUS solver

4. Pressure development case study for a flat plate under the normal applied pressure

Before implementing the formulated pressure model for consolidation of prepregs on a L-shaped tool, the one dimensional through the thickness model is verified for consolidation of prepregs on a flat plate tool subjected to normal applied pressure. Based on the geometry provided in Figure 3, the applied pressure would be carried through the thickness by the fiber bed reinforcement and the hydrostatic and squeeze flow pressure terms developed in the resin and the voids during the consolidation process (see Section 2). As a result, through thickness, one dimensional pressure balance equation could be defined as

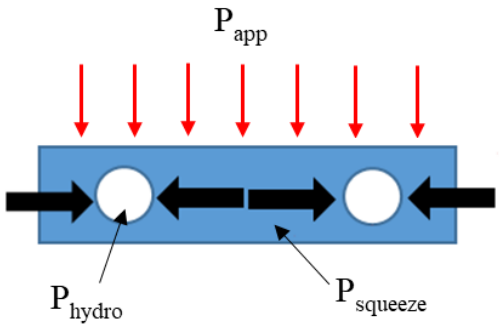

Figure 3. Pressure balance schematic through the thickness

$$P_{app} = E.\mathcal{E} + P_{hydrostatic} + P_{squeeze} \quad (14)$$

Using Eqns. (5-7), Eqn. (14) could be re-written in a form of a non-linear, ordinary differential equation while applied pressure and the strain term are defined as a function of time. For simplicity, as we are using this case only to verify the working of UMAT formulation and Abaqus, we assumed constant temperature condition and no solubility for the voids during the process. Also, modulus of elasticity was defined only through the thickness (E_3) while in-plane elastic modulus (E_1 and E_2) and Poisson ratios were assumed to be inconsequential

$$P_{app}(t) = E_3.\mathcal{E}(t) + \frac{P_0\,\varphi_0}{\varphi_0+\mathcal{E}(t)} + \frac{\eta D^2 {\upsilon_f}^2}{12K_0}\,\frac{1+\mathcal{E}(t)}{\left(1+\mathcal{E}(t)-\upsilon_f\right)^3}\,\dot{\varepsilon} \quad (15)$$

Eqn. (15) can be solved using several numerical techniques using discretization of the strain rate over time. We used first order Euler and fourth order Runge Kutta discretization methods for this study as an example. The solutions were compared with the ABAQUS-UMAT simulation for the flat plate geometry in which identical initial and boundary conditions were applied as E_3=0.1 *GPa*, P_0=100 *KPa*, P_{app}=1 *MPa*, $\varphi_0 = 0.05$, D=0.5 mm, K_0=1E-15 and υ_f=0.6. The comparison between the two methods for flat, 1D simulation and the results attained by the UMAT implemented in ABAQUS solver are shown in Figure 4. The good agreement verifies the accuracy of the implementation of the proposed model in ABAQUS. The negative results for strain obtained from the numerical approach at the very beginning of the process (t<5000 sec) is because the applied pressure was still lower than the assigned initial hydrostatic pressure in the volatiles which led to the expansion rather than the compaction.

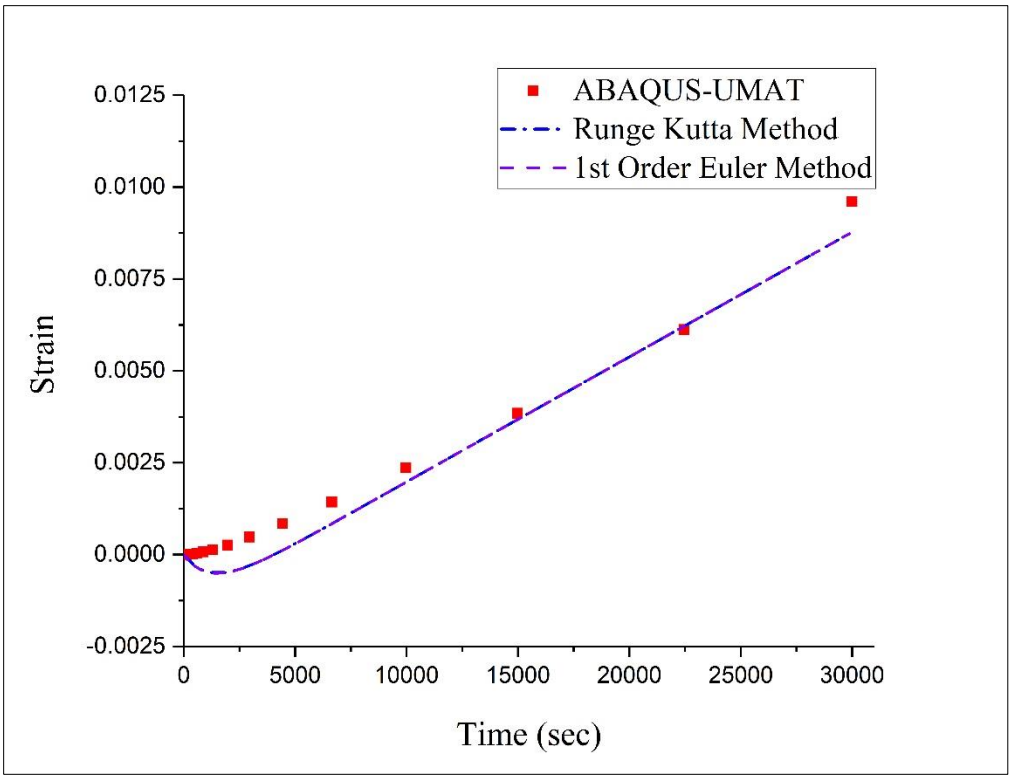

Figure 4. Predicted Strains from the Consolidation Model with Squeeze flow implemented through the thickness and its comparison with the same model implemented in ABAQUS for a flat plate with 5mm thickness.

5. Pressure development model parameters for composite prepregs on curved tool surface

The prepreg layers consisting of viscous resin and fiber reinforcement, are processed at elevated temperature and pressure against the tool surface in a typical autoclave process. During this step, the prepreg layers tend to behave like solid structures and the porosity within the composite will depend on the pressure developed within the resin during the consolidation process as the resin solidifies. The schematic of the L-shaped example modeled with finite element simulation in ABAQUS is shown in Figure 5. The geometry is essentially extruded 2D, but the applied solution is fully three-dimensional.

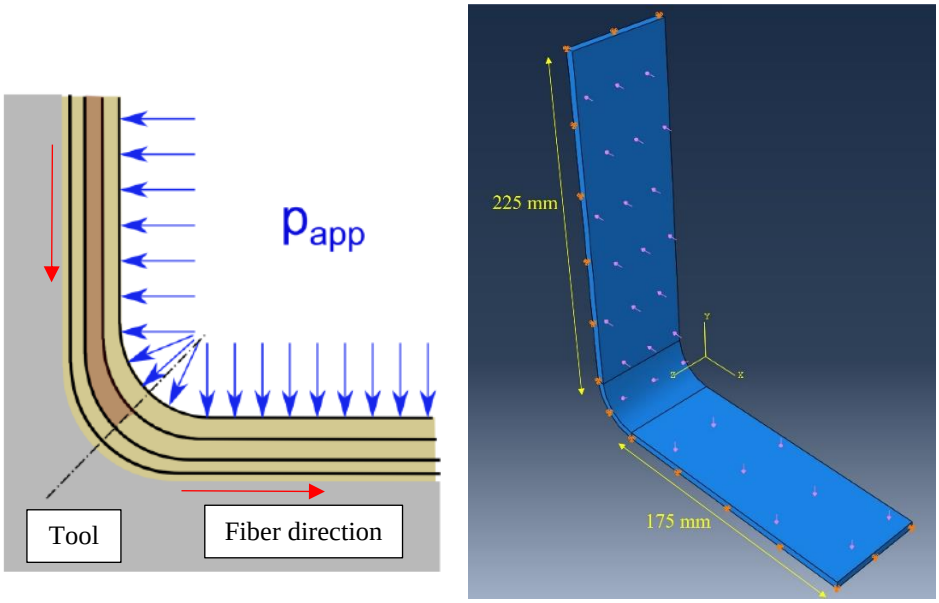

Figure 5. Schematic showing L shaped geometry and applied pressure for an L-shaped part

Based on the flowchart shown in Figure 2, part geometry, material properties and autoclave process are defined in ABAQUS CAE. Two examples containing an assembly of 15 and 28 unidirectional plies are presented. The composite prepreg is modeled as a linear transversely isotropic orthotropic material. Anisotropy ratio with elastic modulus for the fiber direction compared to the transverse direction ($\frac{E_1}{E_2}$ =1000 and 10000) is used in the simulation so that one can address the stacking of unidirectional prepregs. The temperature is assumed to be constant throughout the process and volatile dissolution/diffusion is neglected. Hexahedral, linear standard elements were selected to model the L-shaped geometry. The physical properties and dimensions for the laminates are shown in Table 2.

Table 2. Laminates dimensions and physical properties

L-shaped laminates	Number of plies	Thickness (mm)	Horizontal length (mm)	Vertical length (mm)	Resin viscosity (Poise)
Case 1	15	2.67	175	225	1000
Case 2	28	5	175	225	1000

We will track the variation of pressure with respect to the coordinate system through the thickness from the top surface to the bottom surface for the L-shaped laminate. Thus the coordinate value in the thickness direction is 0 at the top of the top layer and 2.67 mm for the 15

plies and 5 mm for 28 plies laminate at the bottom of the bottom layer in contact with the tool surface.

For the autoclave process, the applied pressure increases linearly with time and reaches 1 MPa at the end of the simulation. The boundary conditions are zero displacement in all direction at the interface of the bottom ply and the tool surface (*Thickness=2.67 mm for 15 plies and 5 mm for 28 plies laminate*). The initial volatile pressure is assumed to be the same as the atmospheric pressure of 100 KPa. Also, initial volatile fraction is varied from 5% to 20% for the parametric study, anisotropy ratio is assumed to be 1000 and 10000 for fiber direction vs in-plane transverse direction and the curvature effect, r_i/h is varied from 3 to 5, where r_i is the radius of the top ply curvature and h is the thickness of the laminate. All the results are obtained at time equals to 30000 sec as the time period used for model simulation which is in line with 8 to 9 hours of autoclave cycle time.

6. Results and discussion

6.1. Resin Pressure Dynamics

During the prepreg consolidation process, two mechanisms are dominant in resisting the applied autoclave pressure during the compaction process: (1) the linear elastic, anisotropic fiber reinforcement and (ii) the resin pressure as a result of the squeeze flow during the process which translates the applied pressure through the plies. However, the reinforcement is very compliant in the transverse direction and stiff in the fiber direction, changing the behavior depending on the surface curvature. Thus, in an L-shaped composite prepreg laminate, two regions must be considered as shown in Figure 6.

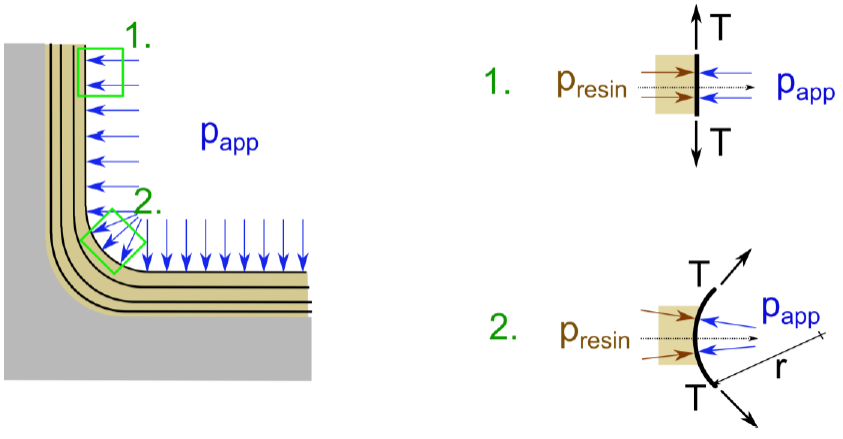

Figure 6. Schematic of how pressure translates between plies in flat and curved regions

In flat parts (zone 1) the transverse stiffness and the resin pressure has to carry all the transverse load as any reinforcement contribution is orthogonal to the normal direction. Once the surface is curved (zone 2), the in-plane tension in the reinforcement (membrane behavior) carries the applied load as well and the other components decrease in accordance with the Terzaghi equation. If the ply-to-ply sliding is prevented, the in-plane tension is "permanent" and depends on the shearing behavior (modulus) of the laminate. If the plies can slide, its character may change to transient dependent on sliding mechanism (viscous, friction, combination…), though for dry friction elastic force corresponding to the frictional resistance will remain. We assumed no sliding in this example. The viscous forces make the situation transient and development must be described as a time dependent function.

The resin pressure contours and normalized resin pressure change with respect to the applied autoclave pressure at the curvature through the thickness are shown in Figure 7a and Figure 8a at time equals to 30000 sec for 5% initial void content in the L-shaped composite laminate with 28 and 15 plies respectively. The final applied pressure is set to 1 MPa at the end of the simulation and the distance between voids, *D* is set to 500 micrometer.

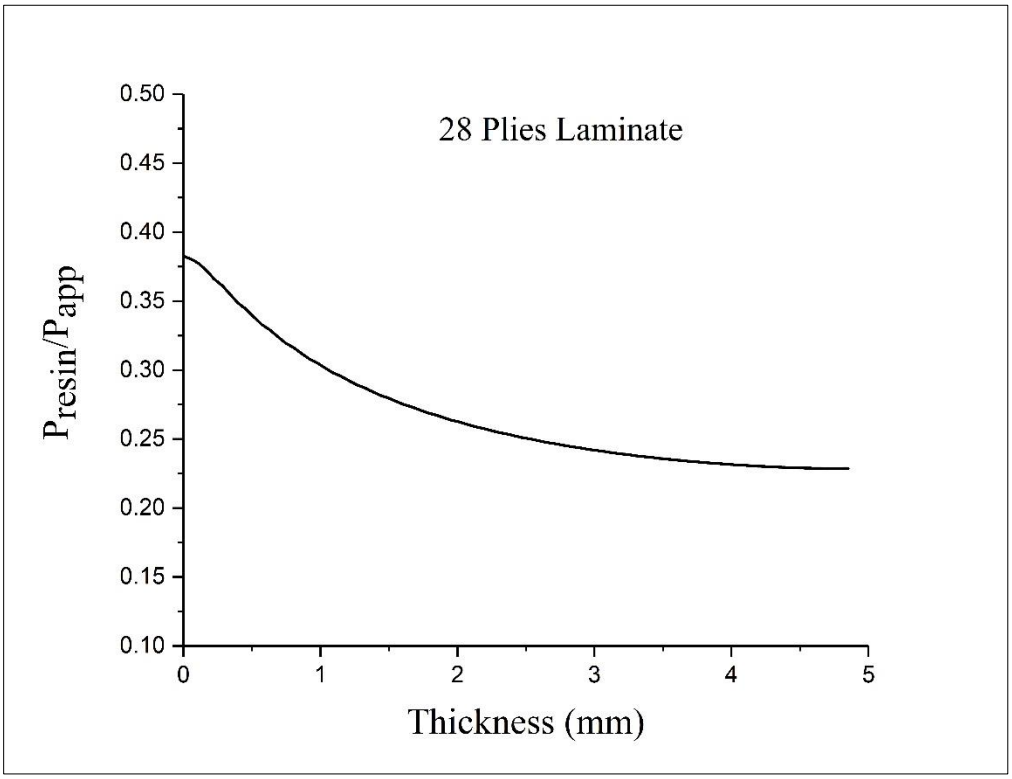

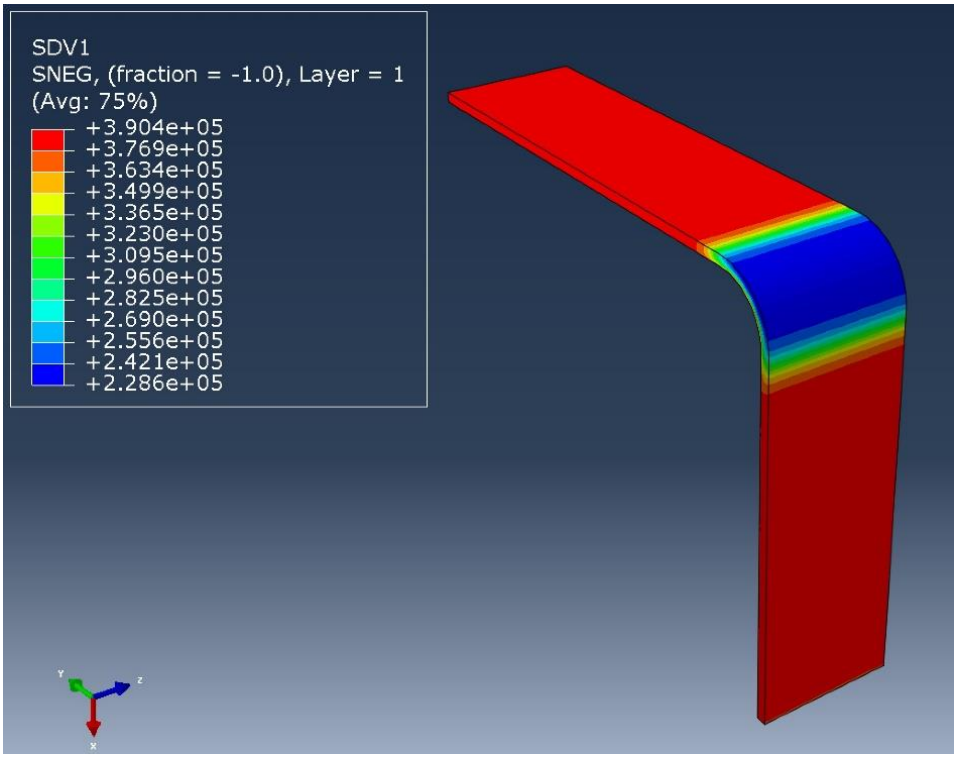

Figure 7. 28 plies laminate with 5% initial void content a) normalized resin pressure distribution with respect to the applied pressure through the laminate thickness at corner b) resin pressure (absolute value) contour for the entire laminate, P_{app}=1MPa, D=500 µm at the end of the simulation, t=30000 sec

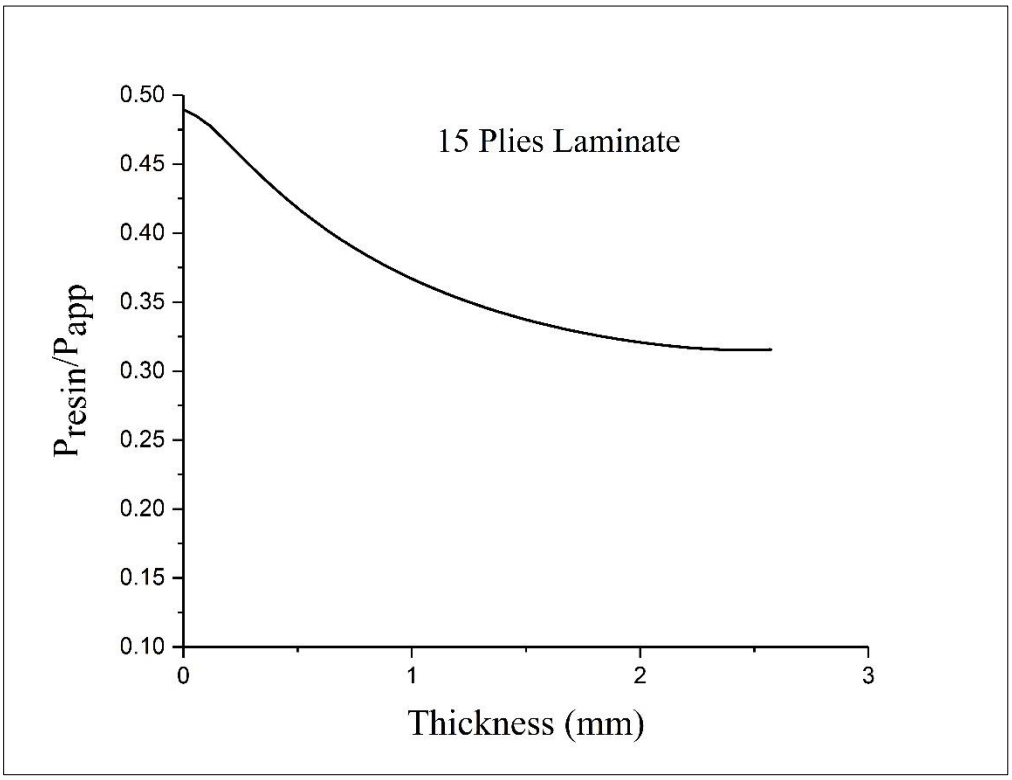

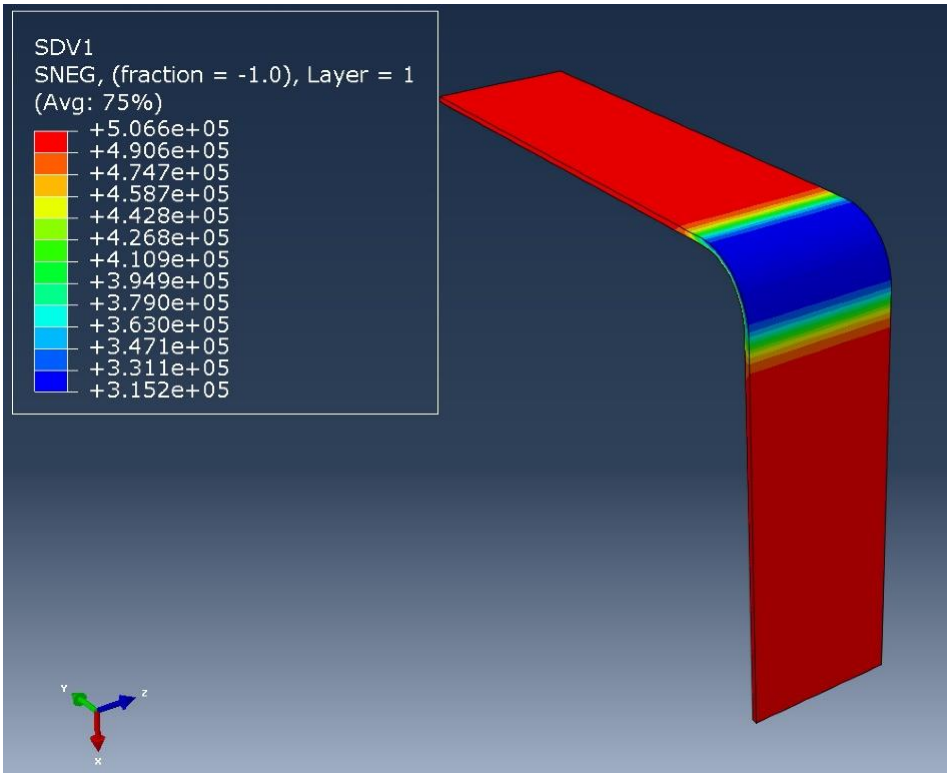

Figure 8. 15 plies laminate with 5% initial void content a) normalized resin pressure distribution with respect to the applied pressure through the laminate thickness at corner b) resin pressure contour for the entire laminate, , P_{app}=1MPa, D=500 µm at the end of the simulation, t=30000 sec

The contour plots in Figures 7b and 8b clearly show the pressure is constant in the thickness direction in the flat section. This pressure is, however, still significantly lower than the applied pressure because the fibrous bed carries part of the load. For the curved regions, the pressure further decreases through the thickness for both laminate thicknesses as the in-plane stress carries additional load there. The reduction in volatile pressure is the main reason for void evolution in the curved region. Two different case studies with different number of plies were used to investigate the effect of thickness on resin pressure drop in the curvature region. It can be observed from the graphs and contours, the resin pressure was higher for the 15 plies laminate compared to the 28 plies laminate at flat and curved regions with respect to the same applied autoclave pressure of 1 MPa.

6.2. Parametric study

In order to illustrate the fiber bed resistance and the hydrostatic pressure vs squeeze flow effects during the compaction process, a parametric study has been performed based on three different initial void fractions and two anisotropy ratios for a layup of 15 and 28 plies. Three

volatile fractions (φ_0) of 5, 10 and 20% are considered in the pressure model (Eqns. 8-10) and for the anisotropy ratio, the extreme cases with large difference between the elasticity in fiber direction versus the transverse direction are used ($\frac{E_1}{E_2}$=1000 and 10000), as the transverse modulus was kept unchanged where the fiber direction modulus was increased accordingly in order to reach the 1000 and 10000 times anisotropy ratio for the simulations. For all parametric studies, final applied pressure was 1 MPa, *D*, the distance between the voids, was maintained at 500 micrometer and the time period for the simulation was 30000 sec. The results for pressure development based on hydrostatic and squeeze flow through the thickness for cases with various void percentage and anisotropy ratio for 28 and 15 plies are shown in Figure 9a and 9b respectively.

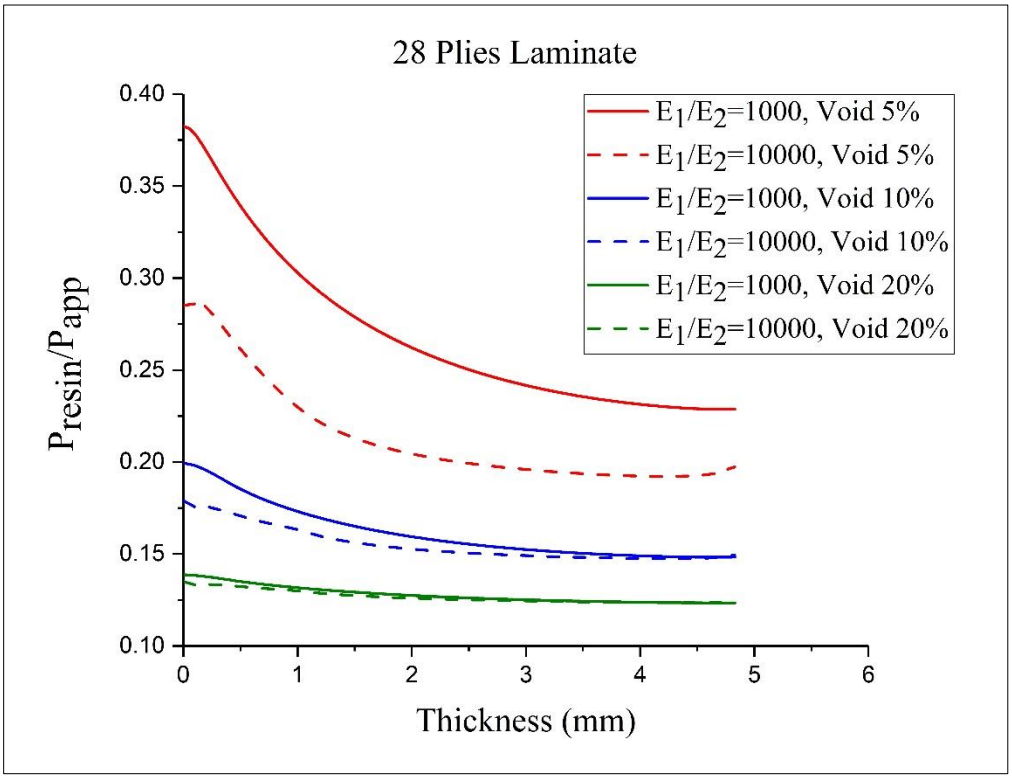

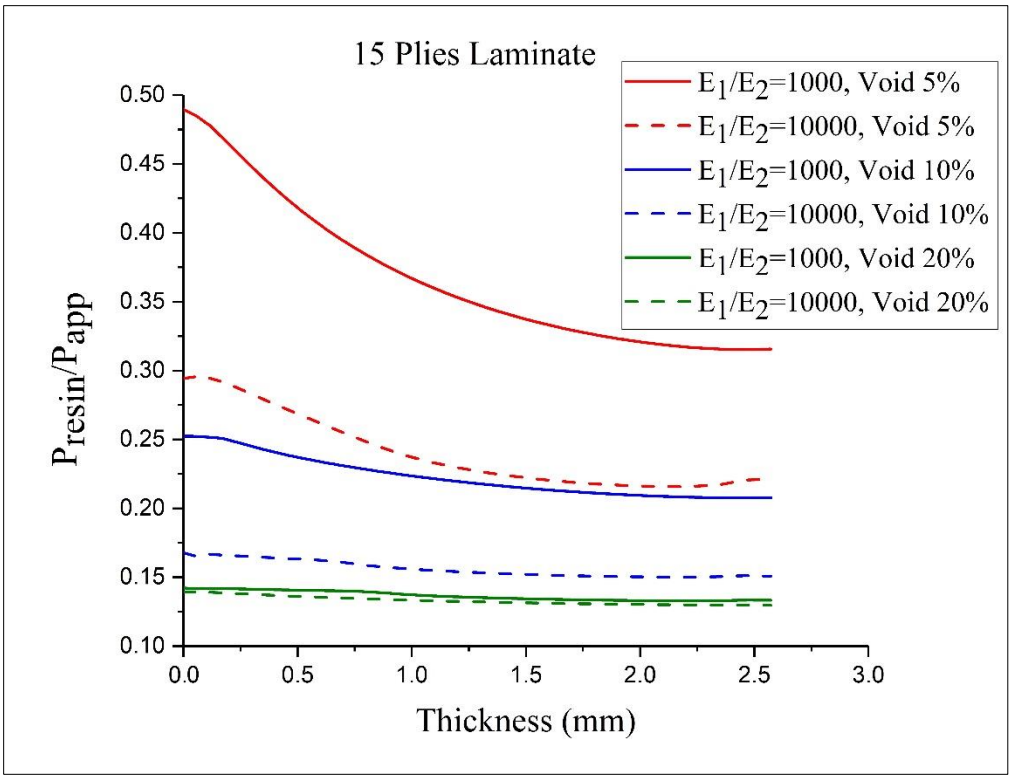

Figure 9. Resin pressure parametric study for different void percentages and anisotropy ratios at corner for (a) 28 plies and (b) 15 plies, final P_{app}=1MPa, D=500 µm and t=30000 sec

As can be observed from the results, highest resin pressure drop across the thickness occurs at lower void content as the 5% void fraction shows highest pressure decrease. Overall, however, the pressure is lower for high porosity as the elastic reinforcement will carry more compaction load than the resin which for higher porosity is more compliant. The effect of the anisotropy ratio is also prominent with lower initial void content percentages becoming less sensitive when the initial void content is higher. In a realistic prepreg laminate, initial porosity is closer to 5% than 20% where the effects of through-thickness pressure drop are much more significant which will promote resin pressure drop in corner regions closer to the tool surface. This effect is more prominently shown in Figure 11 where by reducing the initial void content from 5% to 3 % the void pressure increases up to 75% of the applied load and drops much more quickly. As a result, the pressure model is able to show that for curved regions there is a substantial pressure drop along the thickness and this drop is a strong function of initial void content, anisotropy ratio and the laminate thickness. The void formation and growth around such corners will show larger voids closer to the tool surface than the top surface as seen in Figure 10.

The updated void content was calculated using Eqn. (13) where the bulk strain was obtained from the constitutive model in UMAT implemented in ABAQUS.

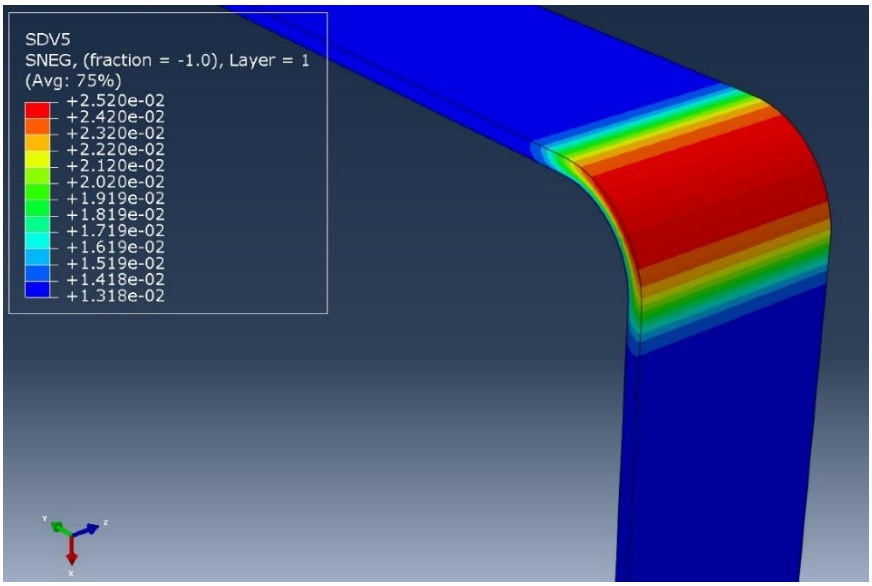

Figure 10. Updated void content distribution contours for 28 plies laminate, initial void=5%, P_{app}=1MPa, D=500 µm and t=30000 sec

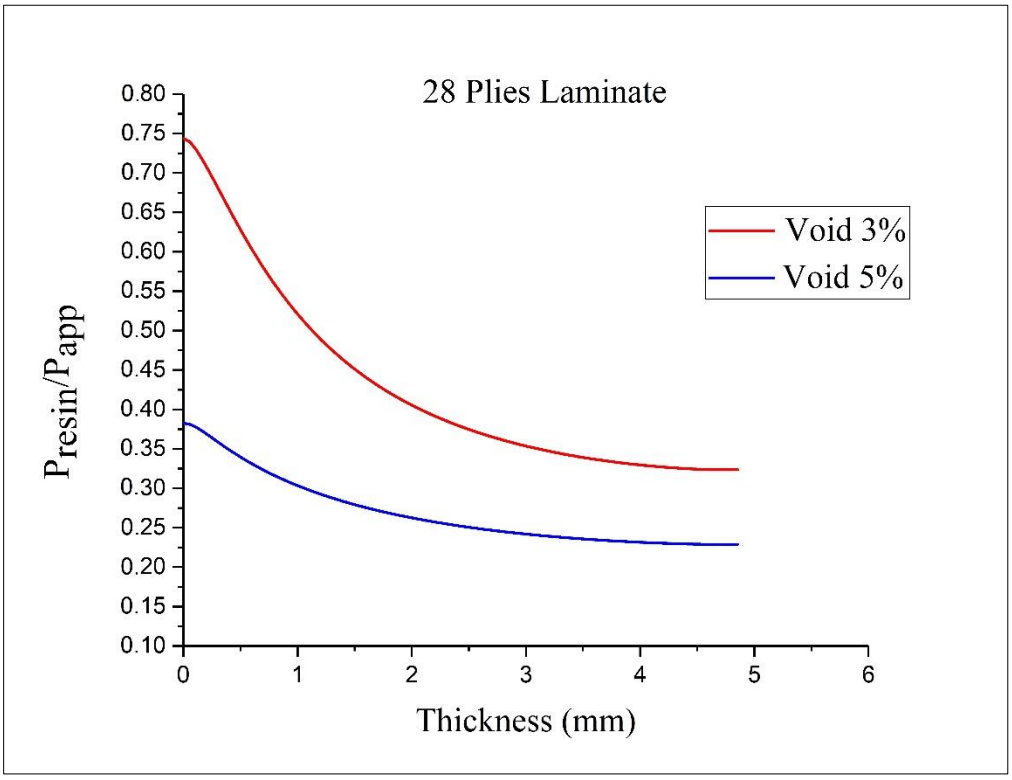

Figure 11. Pressure reduction through the thickness at corner for 28 plies laminate with 3 and 5 % void fraction, for final P_{app}=1MPa, D=500 µm and t=30000 sec

6.3. Applied pressure and geometry effects

The autoclave applied pressure is usually assumed as the value that determines the consolidation. In reality, there are only two extreme cases in which the autoclave applied pressure, after the squeeze flow transient behavior subsides, will equal the pressure within the voids.

First extreme is if the applied pressure is equal to the initial pressure in the voids. In that case, resin pressure will carry all the applied load and the reinforcement will be stress-free and will not deform. This is, obviously, not very useful as no consolidation will take place.

Second extreme is when the applied pressure is very large, the material stiffness of reinforcement becomes negligible and the voids are compressed as the resin roughly carries the entire applied pressure. In this case the voids control the deformation magnitude and the corresponding fiber bed deformation. In that case, the elastic stress in fiber bed is equal to the elastic modulus times the porosity (~bulk strain which is through the thickness). In between these two extremes, however, the steady state pressure in volatiles builds up only to a fraction of the applied pressure as the elastic stress in fiber bed carries part of the compaction load. This depends on two factors:

- The original pressure in the voids.
- The elastic transverse stiffness of the reinforcement.

These behaviors are shown for the case when we assume no squeeze flow for 28 plies laminate in a range of low applied pressure (P_{app}=200 KPa) to extremely large applied pressure (P_{app}=3000KPa) in Figure 12. This clearly shows that the volatile pressure close to the tool surface is just a limited fraction (30-40%) of the applied pressure for the expected consolidation load cases.

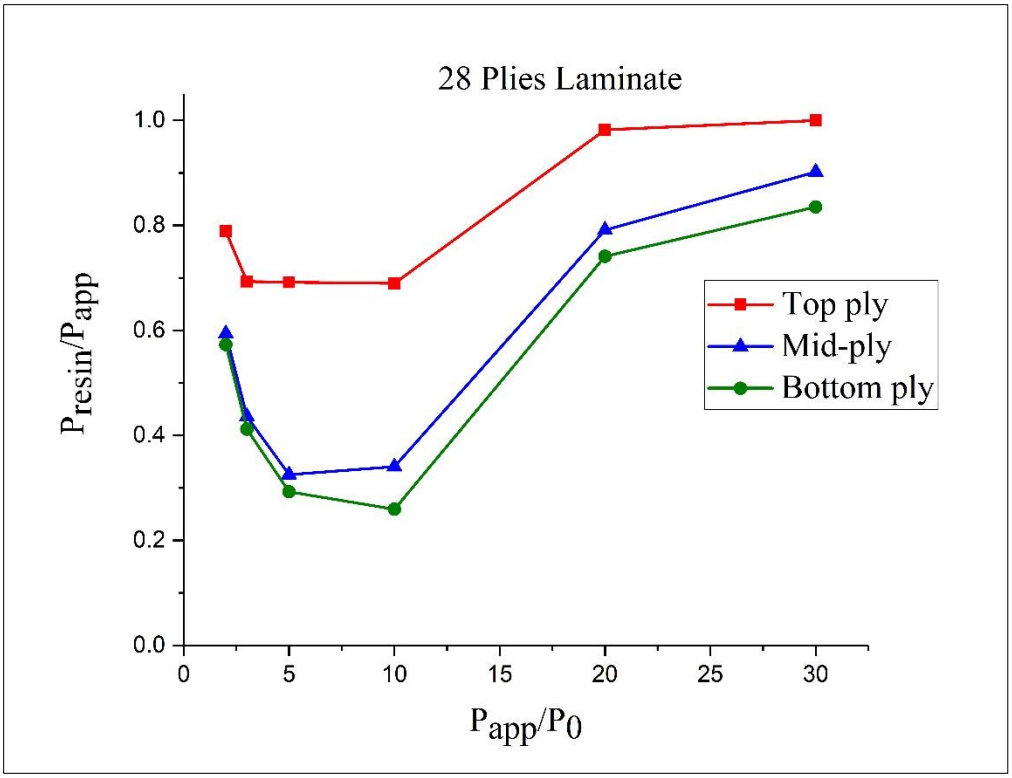

Figure 12. Non-dimensional study exhibiting void pressure variation through the thickness in the corner as the applied pressure is increased to compress the voids for 28 plies laminate with 5% initial void content with no squeeze flow effects, P_{app}=1MPa, D=0 µm and t=30000 sec.

Figure 13 shows this behavior for volatile pressure with respect to the initial void pressure and the applied pressure for the case when we consider squeeze flow effects. In this case the steady state is not reached in 30,000 seconds which leads to additional reduction of pressure within voids. The additional load is carried by the pressure buildup as the resin is squeezed out of the fiber bed. The fraction of applied pressure carried in steady state by the resin decreases until the applied pressure is equal to 10 times the original void pressure, then starts to increase again. Initially the resin pressure is decreasing because the pressure in the voids essentially represents a stiffening non-linear spring, the initial load taken by the voids is much smaller and most of the load is taken by the fibers but as the load increases, voids get more compressed and carry more load relative to the fiber bed (as load carried by fiber bed is limited). The squeeze flow that must fill the voids builds additional resin pressure, effectively reducing the void pressure and stress in fiber bed. If omitted, the relative void pressure in Figure 13 would asymptotically go to 1 for large compression loads. These results were compatible with the assumption of the laminate and the compaction mechanism without sliding, as the layers are

compacted through the thickness. As the plies are extended in fiber direction due to the compaction through thickness, they stretch and build the in-plane stress field which is arrested only in the flat parts by shear stress related to the “sliding” mechanism provided by the laminate shear deformation. Since the ply modulus in the fiber direction is so much higher than the transverse shear modulus, strain in the fiber direction is actually very limited (calculated in a range of 0.1%).

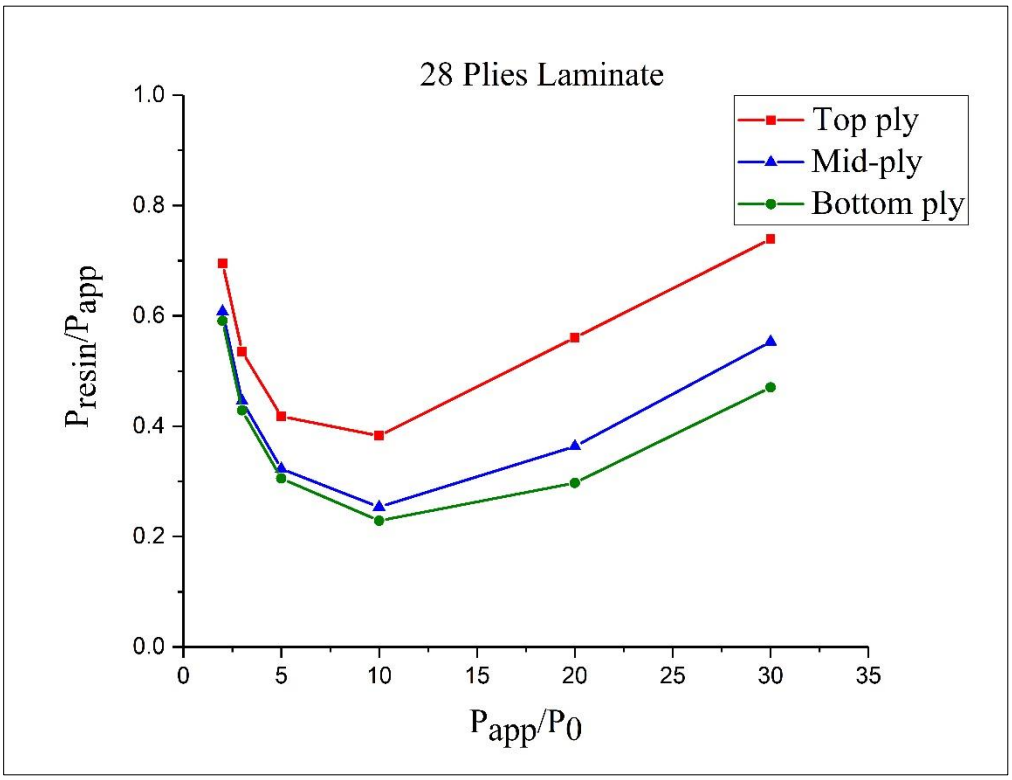

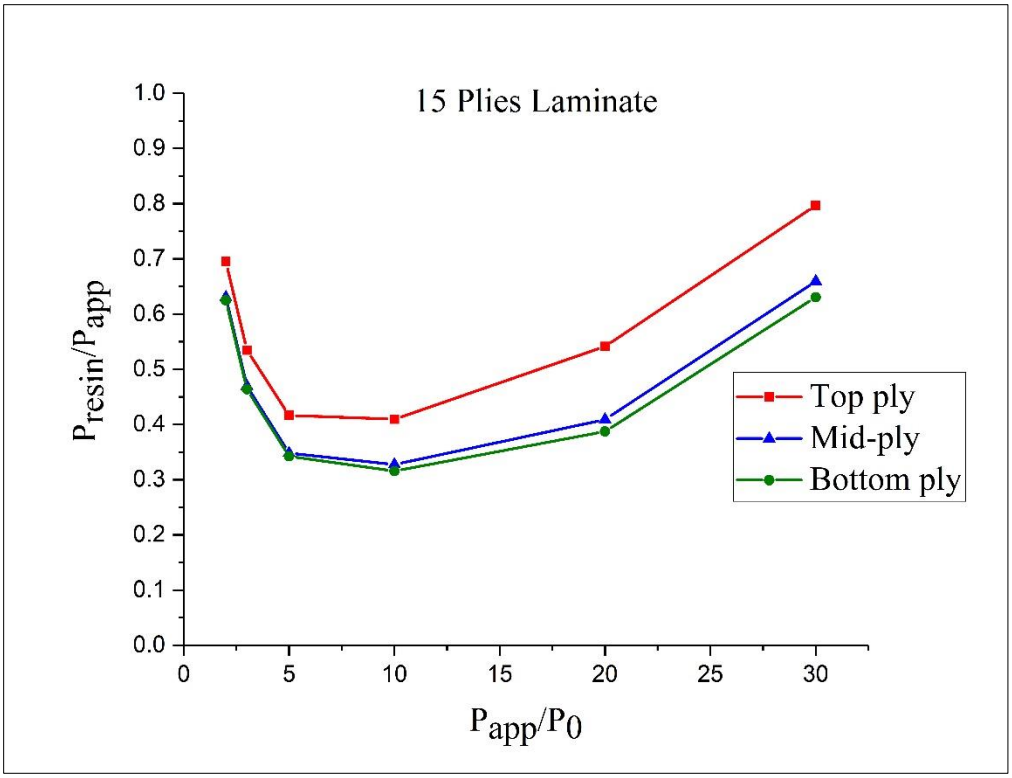

Figure 13. Non-dimensional study exhibiting void pressure variation through the thickness in the corner as the applied pressure is increased to compress the voids for 28 plies and 15 plies laminate with 5% initial void content, P_{app}=1MPa, D=500 µm and t=30000 sec.

The effect of the curvature on the void pressure is shown in Figure 14 for the thicker laminate of 28 plies. Two curvatures' radius over thickness are considered in order to study the effects of sharp curvature on volatile pressure development. As expected, for the 3% and 5% initial void contents, higher pressure drop is experienced for sharper curvatures while the geometry effect is not important for the laminate containing prepregs with initial higher void content of 10%.

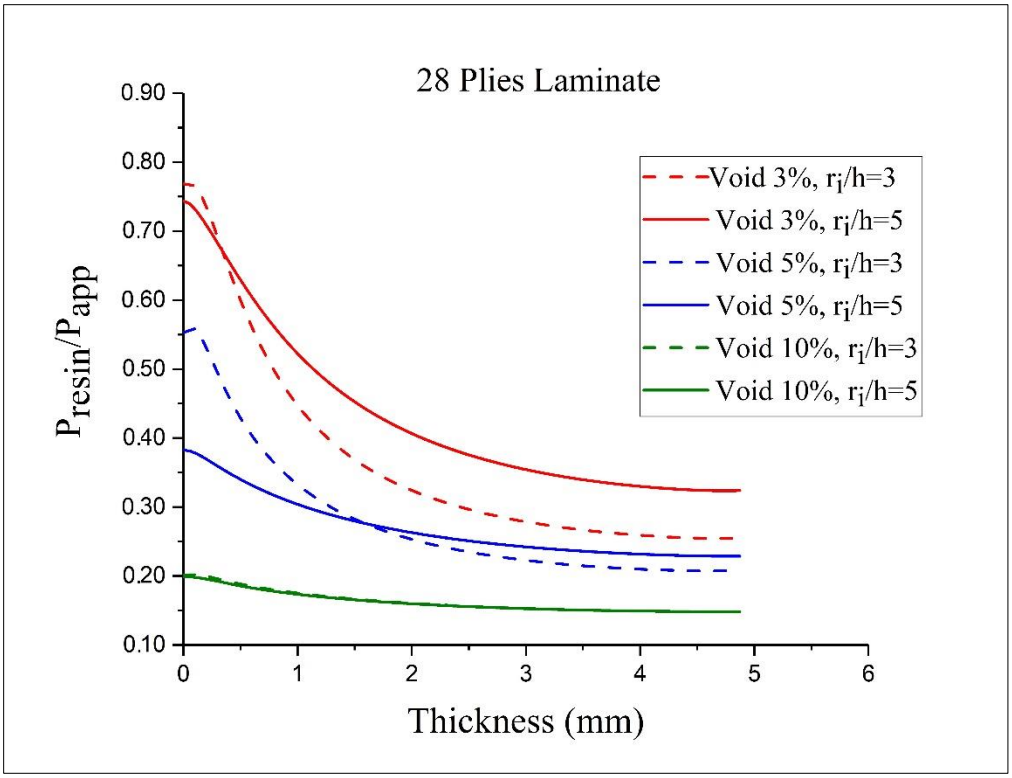

Figure 14. Sharp curvature ($r_i/h=3$) and lower initial void content (3-5%) results in higher pressure drops which will promote more void evolution and movement in the thickness direction at corner, final $P_{app}=1MPa$, D=500 µm and t=30000 sec.

6.4. Stress and strain terms through the thickness

The contours for the stress and strain terms through the thickness for the laminate with 28 plies and 5% void fraction are shown in Figure 15. Based on the result presented for the stress, uniform stress in the normal direction is obtained for the flat surfaces which equals the applied autoclave pressure of 1 MPa. This stress decreases in the region with curvature since the developed pressure is no longer equal to the applied pressure. This is confirmed by the strain results which is around 3.82% as seen in all top surface and the flat areas while the strain decreases to 2.63% in the curvature area which may also give rise to non-uniform thickness around the curve. The results presented in Figure 16 for the 15 plies laminate with the initial void content of 5% show the same pattern for stress and strain contours as what was experienced by the 28 plies laminate.

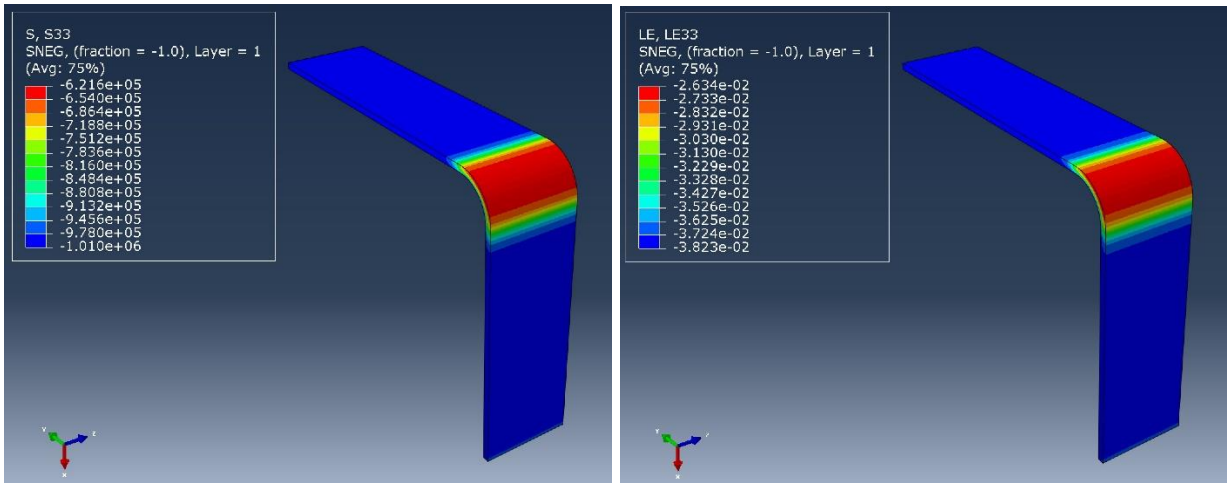

Figure 15. a) Stress, S33 and b) Linear strain results through the thickness for laminate with 5% void content and 28 plies, P_{app}=1MPa, D=500 µ and t=30000 sec.

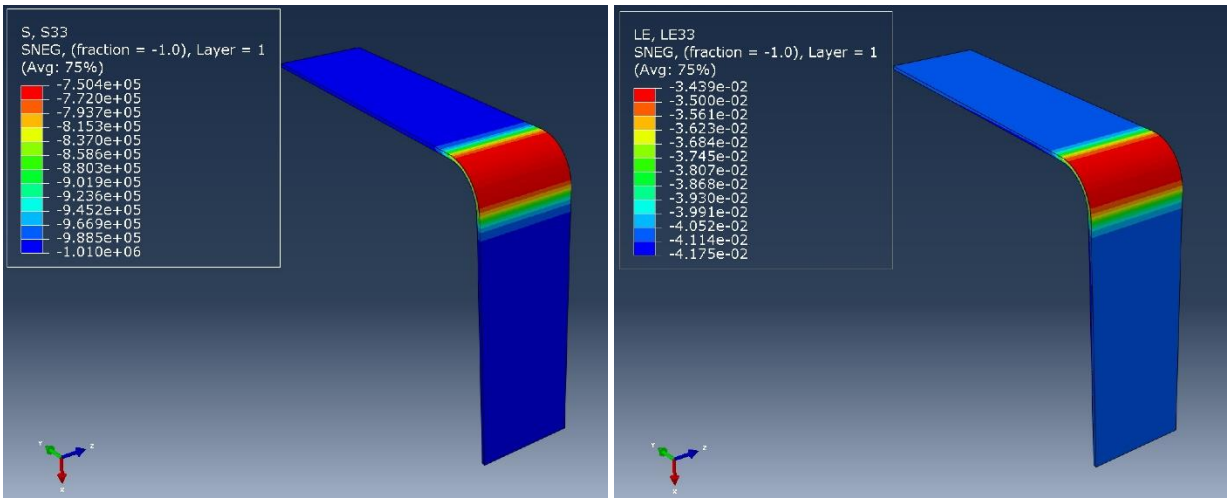

Figure 16. a) Stress, S33 and b) Linear strain results through the thickness for laminate with 5% void content and 15 plies, P_{app}=1MPa, D=500 µm and t=30000 sec.

6.5. Effective mechanisms comparison

As we discussed in section 2 regarding the effects of all dominant mechanisms on volatile pressure development, presented in Figure 17 is each term's effect in qualitative format for the 28 plies laminate under 1 MPa applied pressure at 30000 sec for the consolidation process. Based on the results shown, compression stress in the fibrous reinforcement is the most significant term in transferring the applied pressure. For real materials, this value may vary significantly depending on the initial fiber volume fraction and reinforcement architecture. The squeeze flow effect is the least significant term at this time and should drop to zero if the load remains constant and the time is long enough. Note that during the pressure development at earlier times this is not

necessarily true, in case shorter cycles are explored. The summation of all terms at the top ply (*thickness=0*) is practically equal to 1 MPa or the applied autoclave pressure while the effect of each term shrinks when we reach the bottom ply close to the tool surface. The membrane in-plane stress is responsible for this reduction as it reacts more and more of the applied load.

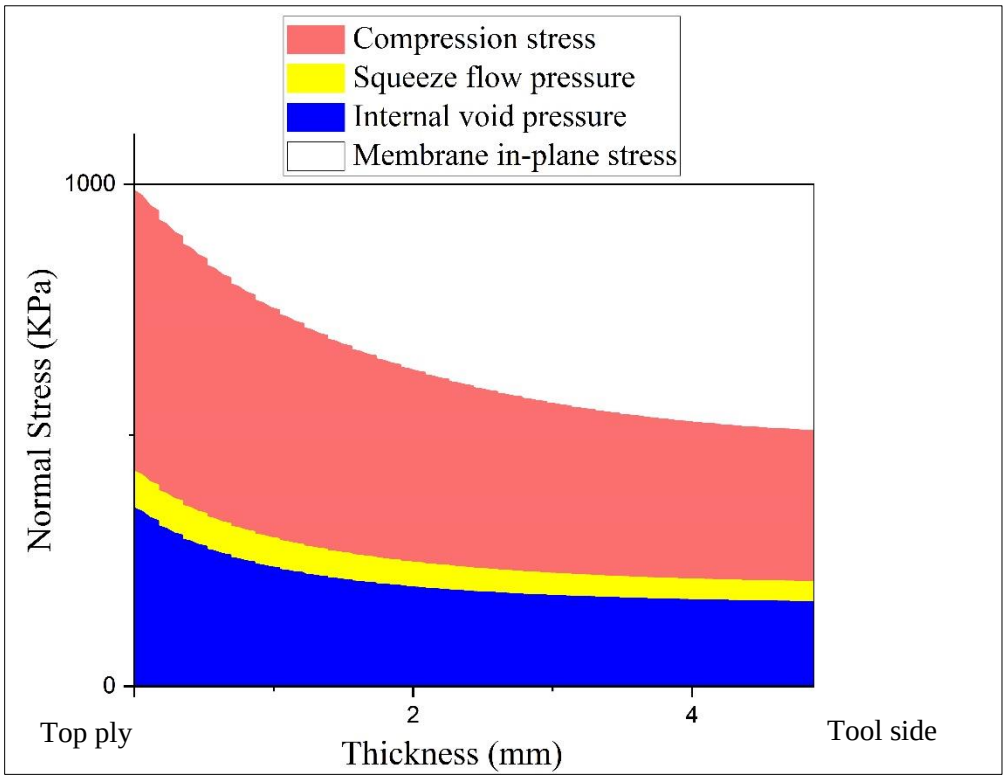

Figure 17. How the various pressure terms vary across the thickness for 28 plies laminate with 5% initial void content, P_{app}=1MPa, D=500 µm and t=30000 sec.

7. Summary and Conclusion

In this study, a new constitutive model has been developed as a UMAT subroutine for the finite element package ABAQUS/Standard to study the resin pressure dynamics during the consolidation process for prepregs with varying initial void content. Most significant simplification is that of the constant temperature. The fiber bed model is defined based on the linear anisotropic behavior of the composite laminate. The volatile "hydrostatic" pressure is based on ideal gas law and the resin pressure due to squeeze flow is described by substituting "effective" void spacing and fiber bed permeability into one-dimensional model. The initial void content is assumed to be uniform. The permeability variation is based on Karman-Kozeny equation. A parametric study is conducted in which the role of the anisotropic fiber behavior in

addition to the initial void hydrostatic pressure and the induced resin squeeze flow due to compaction are considered during the consolidation process in the autoclave. The resin pressure during the consolidation process has been predicted through the thickness for an L-shaped laminate.

The results show that the applied pressure is never reached in the resin as the elastic resistance of fiber bed carries some load. More importantly, there is an additional – and very significant - reduction in the resin pressure at the curvature region near the corner of the L shape whereas the rest of the flat area exhibits a uniform pressure distribution. The reduction in resin pressure through the thickness will promote the void growth as the resin pressure drops from the top surface to the tool surface non-uniformly. The pressure results were confirmed by the stress and strain terms for thin and thick laminates. A non-uniform pressure state in the corner extends to the elastic stress and strains and this indicates that the laminate may undergo thickness change in the curved region. Lower initial void content, thicker laminates, higher anisotropy and sharper curvatures seems to show the highest pressure drop in the resin and hence higher probability of void movement and growth in addition to non-uniform thickness in the curved region. The parametric study demonstrates the ability of the model in simulating various case studies to model the void evolution during the consolidation process.

Acknowledgement

This work is supported by Composites Automation, LLC and the United States Naval Air and Warfare Center under Prime Contract No. N68335-17-C-0093 administrated by Dr. Suresh G. Advani. The views, opinions and/or findings contained in this report are those of the author(s) and should not be construed as an official US Naval Air Warfare Center position, policy or decision unless so designated by other documentation. The authors also declare that they have no conflict of interest.

References

1. Chandrakala K, Vanaja A, Rao R (2009) *Storage life studies on RT cure glass—epoxy prepregs*. J Reinf Plast Compos 28(16):1987– 1997.
2. Herrmann A, Zahlen P, Zuardy I (2005) *Sandwich structures technology in commercial aviation*. In: Thomsen OT, Bozhevolnaya E, Lyckegaard A (eds) Sandwich structures 7: advancing with sandwich structures and materials. Springer Netherlands, pp 13–26.

3. Kardos J. L., Duduković M. P., Dave R. (2005) *Void growth and resin transport during processing of thermosetting — Matrix composites.* Epoxy Resins and Composites IV. Advances in Polymer Science, vol 80. Springer.
4. Lightfoot SC, Wisnom MR, Potter K., (2013) *A new mechanism for the formation of ply wrinkles due to sheer between plies*. Composites Part A, 49:139–147.
5. Potter K, Khan B, Wisnom MR, Bell T, Stevens J (2008) *Variability, fiber waviness and misalignment in the determination of the properties of composite materials and structures*. Composites Part A, 39:1343–1354.
6. Bloom LD, Wang J, Potter KD (2013) *Damage progression and defect sensitivity: an experimental study of representative wrinkles in tension*. Composites Part B 45:449–458.
7. Hsiao HM, Daniel IM (1996) *Effect of fiber waviness on stiffness and strength reduction of unidirectional composites under compressive loading*. Compos Sci Technol 56:581–593.
8. Garnich MR, Karami G (2004) *Finite element for stiffness and strength of wavy fiber composites*. J Compos Mater 38(4):273–292.
9. Karami G, Garnich MR (2005) *Effective moduli and failure consideration for composites with periodic fiber waviness*. Compos Struct 67:461–475.
10. Hubert P, Poursartip A (1998) *A review of flow and compaction modelling relevant to thermoset matrix laminate processing*. J Reinf Plast Compos 17(4):286–318.
11. Fernlund G, Griffith J, Courdji R, Poursartip A (2002) *Experimental and numerical study of the effect of caul-sheets on corner thinning of composite laminates*. Composites Part A, 33(3):411–426.
12. Naji MI, Hoa SV (2000) *Curing of thick angle-bend thermoset composite part: curing process modification for uniform thickness and uniform fiber volume fraction distribution*. J Compos Mater 34(20):1710–1755.
13. Li Y, Li M, Gu Y, Zhang Z (2009) *Numerical and experimental study on the effect of lay-up type and structural elements on thickness uniformity of L-shaped laminates*. Appl Compos Mater 16(2): 101–115.
14. Wang X, Zhang Z, Xie F, Li M, Dai D, Wang F (2009) *Correlated rules between complex structure of composite components and manufacturing defects in autoclave molding technology*. J Reinf Plast Compos 28(22):2791–2803.
15. Li M (2001) *Optimal curing of thermoset composites: thermochemical and consolidation considerations*. PhD Thesis, University of Illinois at Urbana-Champaign.
16. Mélanie B (2010) *Out-of-autoclave manufacturing of complex shape composite laminates*. McGill University, Montreal, Manufacturing.
17. Xin CB, Gu YZ, Li M, Luo J, Li YX, Zhang ZG (2011) *Experimental and numerical study on the effect of rubber mold configuration on the compaction of composite angle laminates during autoclave processing*. Composites Part A, 42 (10):1353–1360.
18. Johnston A (1997) *An integrated model of the development of process-induced deformation in autoclave processing of composite structures*. Ph.D. thesis, The University of British Columbia.
19. Hubert P, Vaziri R, Poursartip A (1999) *A two-dimensional flow model for the process simulation of complex shape composite laminates*. Int J Numer Meth Eng 44(1):1–26 86.
20. Min L, Yanxia L, Yizhuo G (2008) *Numerical simulation flow and compaction during the consolidation of laminated composites*. Wiley Intersci Soc Plast Eng 29(5):560–568 87.
21. Dave R, Kardos JL, Dudukovic MP (1987) *A model for resin flow during composite processing: part 1-general mathematical development*. Polym Compos 8(1):29–38 88.

22. Gutowski TG, Cai Z, Bauer S, Boucher D (1987) *Consolidation experiments for laminate composites*. J Compos Mater 21(7):650–669 89.
23. Li M, Li Y, Zhang Z, Gu Y (2008) *Numerical simulation flow and compaction during the consolidation of laminated composites*. Polym Compos 29(5):560–568 90.
24. Li M, Charles L, Tucker III (2002) *Modelling and simulation of two-dimensional consolidation for thermoset matrix composites*. Compos A 33:877–892 91.
25. Dong C (2011) *Model development for the formation of resin-rich zones in composites processing*. Compos A 42:419–424.
26. Simacek, P., Advani, S.G., Gruber, M., Jensen, B. (2013), *A non-local void filling model to describe its dynamics during processing thermoplastic composites*, Composites Part A, 46 (1), 154-165.